Cylindrical Langmuir probes beyond the orbital-motion-limited regime

R. D. Estes
Harvard-Smithsonian Center for Astrophysics, 60 Garden St., Cambridge, Massachusetts 02138

J. R. Sanmartín[a)]
Escuela Técnica Superior de Ingenieros Aeronáuticos, Universidad Politécnica de Madrid, 28040 Madrid, Spain

(Received 5 April 2000; accepted 12 June 2000)

The current I to a cylindrical probe at rest in an unmagnetized plasma, with probe bias highly positive, is determined. The way I lags behind the orbital-motion-limited (OML) current, $I_{\mathrm{OML}} \propto R$, as the radius R exceeds the maximum radius for the OML regime to hold, is of interest for space-tether applications. The ratio I/I_{OML} is roughly a decreasing function of $R/\lambda_{\mathrm{De}} - R_{\max}/\lambda_{\mathrm{De}}$, which is independent of bias, with λ_{De} the electron Debye length and $R_{\max}/\lambda_{\mathrm{De}}$ roughly an increasing function of the temperature ratio, T_i/T_e. The dependence of current on ion energy is used to discuss the effect of probe motion through the plasma, a case applying to tethers in low orbit.
 [S1070-664X(00)00210-X]

I. INTRODUCTION

The interaction of conductive space tethers with the magnetized ionosphere has potential applications that range from power generation and propulsion (or drag for deorbiting purposes),[1,2] to the use of wave and particle emissions.[3–5] The basic problem is how to collect ionospheric electrons: The small electron gyroradius and Debye length could greatly reduce collection through magnetic guiding and electric shielding. Using the thin tether itself (left bare over kilometers of its length) as the anode offers the benefits of (1) passive electron collection over a large area with no shielding or magnetic effects[6] and (2) relative insensitivity to regular drops in plasma density along its orbit.[7] A National Aeronautics and Space Administration experiment (Propulsive Small Expendable Deployer System) will test bare-tether collection this year in a Delta-2 orbital flight. Bare tethers are being considered for reboost of both the Russian MIR and the International Space Stations, as well as for future use in the Jovian system.

A bare tether collects current as a cylindrical Langmuir probe. The electron current I to a long cylinder at rest in a collisionless, unmagnetized, Maxwellian plasma of density N_∞ and temperatures T_e and T_i, may be written as

$$I = I_{\mathrm{th}} \times \text{a function of } e\Phi_P/kT_e,\ R/\lambda_{\mathrm{De}},\ T_i/T_e,$$

where $I_{\mathrm{th}} \equiv 2\pi RL \times eN_\infty \times \sqrt{kT_e/2\pi m_e}$ is the random current, λ_{De} is the Debye length, and R, L, and Φ_P are probe radius, length, and bias. For cylinders thin enough, however, I/I_{th} only depends on $e\Phi_P/kT_e$. This is the orbital-motion-limited (OML) regime; at high bias ($e\Phi_P/kT_e \sim 10^3$ for a typical tether) one has

$$I_{\mathrm{OML}} \approx I_{\mathrm{th}} \times \sqrt{4e\Phi_P/\pi kT_e} = 2RLeN_\infty \sqrt{2e\Phi_P/m_e} \quad (e\Phi_P \gg kT_e). \tag{1}$$

Actually, this equation is also valid for a noncircular cross section if convex enough, with $1/\pi$ times its perimeter replacing $2R$ above.[8]

Since I_{OML} is proportional to radius (or perimeter) of the cross section, a large current may require a large radius; if this is too large, however, the current I will not reach the OML value because of electrical effects. The maximum radius $R_{\max}$ for the OML regime to hold with other parameters fixed was determined recently.[9] The maximum width of a thin tape and conditions to have negligible effects from the magnetic field, and from electrons trapped in bounded orbits, were also established in Ref. 9. Here we study the way I/I_{OML} drops below unity when R goes above $R_{\max}$ at very high bias, a matter of interest for the design of bare tethers. In Sec. II we recollect the basic structure of the analysis in Ref. 9, and point out the new features of the present problem. In Sec. III we describe the scheme to calculate the current. In Sec. IV we discuss results on I/I_{OML}; its dependence on $R_{\max}$, which varies with plasma parameters; and the effect of tether motion relative to the ionosphere.

II. STRUCTURE OF THE POTENTIAL

In general, determining electron trajectories to obtain the collected current I requires solving Poisson's equation for $\Phi(r)$

$$\frac{\lambda_{Di}^2}{r}\frac{d}{dr}r\frac{d}{dr}\left(\frac{e\Phi}{kT_i}\right) = \frac{N_e}{N_\infty} - \frac{N_i}{N_\infty} \approx \frac{N_e}{N_\infty} - \exp\left(-\frac{e\Phi}{kT_i}\right), \tag{2}$$

with boundary conditions $\Phi = \Phi_P > 0$ at $r = R$, $\Phi \to 0$ as $r \to \infty$. The Boltzmann law used for the ion density N_i is quite accurate at the high bias of interest. Regarding N_e, since the Vlasov equation conserves the distribution function $f_e(\mathbf{r},\mathbf{v})$ along orbits, and trapped electrons may be ignored,[9] we have

a)Electronic mail: jrs@faia.upm.es

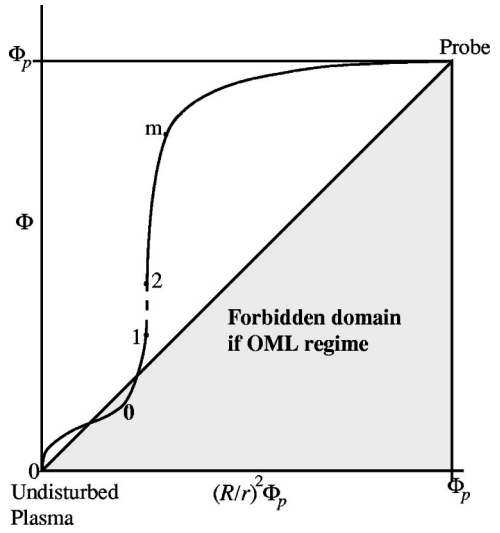

FIG. 1. Schematics of potential Φ vs $\Phi_P R^2/r^2$ for $R>R_{\max}$ (maximum radius for the OML regime to hold). The plasma is quasineutral below point 1, with no potential barriers below point 0. The ratio $\Phi r^2/\Phi_P R^2$ reaches a large maximum at a point m in the ion-free, broad region above thin, nonquasineutral layers at points 1 and 2.

$f_e(\mathbf{r},\mathbf{v})=f_{eM}(v_\infty)$ (undisturbed Maxwellian) if the $\mathbf{r},\mathbf{v}$ orbit traced back in time reaches infinity and $f_e(\mathbf{r},\mathbf{v})=0$ otherwise.[10] Since energy is also conserved and f_{eM} is isotropic, values for $\mathbf{r},\mathbf{v}$ determine the value of f_{eM} in terms of the local potential $\Phi(r)$.

Both density N_e at any radius r and current I can then be written as integrals of f_{eM} over axial velocity and (allowed ranges of) angular momentum J and energy E in the perpendicular plane, which are all three conserved. Defining

$$J_r(E)\equiv\sqrt{2m_e r^2[E+e\Phi(r)]}, \tag{3}$$

$$J_r^*(E)\equiv\text{minimum}\ \ [J_{r'}(E);r'\geqslant r], \tag{4}$$

one finally arrives at[9]

$$\frac{N_e}{N_\infty}=\int_0^\infty\frac{dE}{\pi kT_e}\exp\left(\frac{-E}{kT_e}\right)\times\left[2\sin^{-1}\frac{J_r^*(E)}{J_r(E)}-\sin^{-1}\frac{J_R^*(E)}{J_r(E)}\right], \tag{5}$$

$$I=\frac{2LeN_\infty}{m_e}\times\int_0^\infty\frac{dE}{kT_e}\exp\left(\frac{-E}{kT_e}\right)J_R^*(E). \tag{6}$$

For given r and E, values $J=0$ and $J=J_r(E)$ correspond to zero azimuthal and radial velocities, respectively. In case we have $J_r^*(E)<J_r(E)$, inward trajectories in the range $J_r^*(E)<J<J_r(E)$ are unpopulated; such electrons, if traced back in time, turn around at radii between r and the (larger) radius where the minimum in (4) occurs: There is a barrier in the radial effective potential energy. Note that N_e is a functional of the full potential structure rather than a function of its local value. That structure, as determined in Ref. 9, can be illustrated by schematically displaying Φ versus $\Phi_P R^2/r^2$, with the ordinate-to-abscissa ratio proportional to $r^2\Phi$ (Fig. 1).

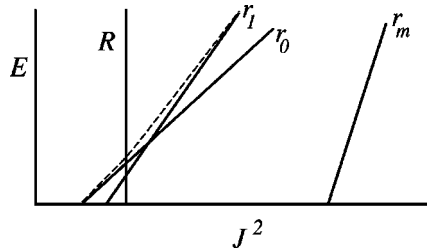

FIG. 2. Straight lines in the E (energy) vs J^2 (squared angular momentum) plane, for the r-family defined in Eq. (10), $J^2=J_r^2(E)$. Shown are r-lines for the probe and for points m, 1, and 0 in Fig. 1, as well as the envelope of lines in the r_0-r_1 range.

The faraway quasineutral solution to (2), $N_e\approx N_i$, behaves as $\Phi\sim 1/r$. As one moves up on the profile from the origin in the figure, $r^2\Phi(r)$ decreases to a minimum at some radius r_0. The quasineutral solution remains valid further above, up to a point 1 where $-d\Phi/dr$ diverges. Above point 1 there are two thin nonquasineutral layers that take the solution to values $\Phi_1\ll\Phi\ll\Phi_P$, and to a radius r_2 a bit closer to the probe; points 0–1 if drawn to scale would lie very close to the origin in Fig. 1 because $e\Phi_0$ and $e\Phi_1$ are of order of kT_i whereas $e\Phi_P/kT_i$ is very large. In the broad region between radii r_2 and R the ion density is negligible, and $r^2\Phi(r)$ reaches a large maximum at some point m before dropping to $R^2\Phi_P$ at the probe.

Note in Eqs. (3) and (4) that, for any particular r, having $J_r^*(0)=J_r(0)$ suffices to make $J_r^*(E)$ equal to $J_r(E)$ for all $E\geqslant 0$; using $J_r^2(0)\propto r^2\Phi(r)$, the no-barrier condition reads

$$r'^2\Phi(r')\geqslant r^2\Phi(r),\quad r'\geqslant r. \tag{7}$$

Since we have

$$d(r^2\Phi)/dr>0,\quad r>r_0, \tag{8}$$

there are energy barriers at no radius below point 0 in Fig. 1

$$J_r^*(E)=J_r(E)\quad\text{for}\ \ E\geqslant 0\quad(r\geqslant r_0). \tag{9}$$

Again, this can be illustrated by depicting the structure of the r-family of straight lines

$$J^2=J_r^2(E)\quad\text{or}\ \ E=\frac{J^2}{2m_e r^2}-e\Phi(r), \tag{10}$$

in the J^2-E plane (Fig. 2). The line slope steepens monotonically as r decreases, moving up in Fig. 1, while the foot, $J^2(E=0)$, varies as $r^2\Phi(r)$. Property (8) means that, throughout the range $r>r_0$, the r-line moves to the left in Fig. 2 for all positive energies. Past point 0, however, the line foot moves back to the right. Since we have $r_1^2\Phi_1>r_0^2\Phi_0$ and $r_1<r_0$, the r_0- and r_1-lines meet at some positive energy, resulting in an r-dependent energy range with effective potential energy barriers.

The envelope $J^2=J_{\text{env}}^2(E)$ of lines in the range $r_1<r<r_0$ is determined by the equations $J^2-J_r^2(E)=0$, $\partial[J^2-J_r^2(E)]/\partial r=0$, yielding the parametric representation

$$J^2=J_{\text{env}}^2(r)\equiv-m_e r^3 e d\Phi/dr, \tag{11a}$$

$$E=E_{\text{env}}(r)\equiv-e\Phi(r)-re d\Phi/dr. \tag{11b}$$

The envelope lies to the left of all lines in that range, touching each line at the point given by Eqs. (11a) and (11b); it leaves the r_0-line at $E=0$,[11] and reaches the r_1-line asymptotically, as $E_{\rm env}$ and $J^2_{\rm env}$ diverge with $-d\Phi/dr$ as $r\to r_1$ (Fig. 2). For each radius between r_0 and r_1 only that part of the envelope below the touching point enters in the determination of $J_r^*(E)$; we would thus have $J_r^*(E)=J_{\rm env}(E)$ for $E<E_{\rm env}(r)$, and $J_r^*(E)=J_r(E)$ otherwise. As r approaches r_1, however, $E_{\rm env}(r)$ diverges making $J_r^*(E)=J_{\rm env}(E)$ valid for all energies. As Φ rises rapidly with decreasing r above point 1 in Fig. 1, the line foot in Fig. 2 moves far to the right, the line itself steepening moderately. Within thin layers and broad region we would then have

$$J_r^*(E)=J_{\rm env}(E) \quad \text{for } E\geqslant 0 \quad (r\leqslant r_1). \tag{12}$$

At point m in Fig. 1, the line foot turns again to the left, finally ending at the R-line (Fig. 2), which is near-vertical ($R\ll r_1, E\sim kT_e\ll e\Phi_P$), and has its foot to the right of the envelope, corresponding to point 0 lying below the diagonal in Fig. 1. Clearly, Eq. (12) fails in some neighborhood of the probe. At R in particular, we have

$$J_R^*(E)=J_{\rm env}(E) \quad \text{for } 0<E<E_c, \tag{13a}$$

$$J_R^*(E)=J_R(E) \quad \text{for } E>E_c, \tag{13b}$$

with E_c the energy at the crossing of envelope and R-line; this results in a ratio $I/I_{\rm OML}<1$, or $R>R_{\max}$. Note that maximum (OML) current in (6) would only occur with $J_R^*(E)=J_R(E)$ for all energies (no effective energy barrier for R), a condition requiring, according to (7)

$$r^2\Phi(r)\geqslant R^2\Phi_p, \quad r\geqslant R. \tag{14}$$

Point 0 would then lie at or above the diagonal in Fig. 1, and the entire R line would appear to the left of the envelope in Fig. 2 ($R\leqslant R_{\max}$); with $E\ll e\Phi_P$ we would have $J_R(E)\approx J_R$ (0), (6) then recovering Eq. (1) for the high-bias OML law.

III. CALCULATION OF CURRENT

Using (1) and (6), the ratio $I/I_{\rm OML}$ takes the form

$$\frac{I}{I_{\rm OML}}=\int_0^\infty \frac{dE}{kT_e}\exp\left(\frac{-E}{kT_e}\right)\frac{J_R^*(E)}{J_R(0)}, \tag{15}$$

with $J_R^*(E)$ given by Eqs. (13a) and (13b), and $J_R(E)=J_R(0)=\sqrt{2m_eR^2e\Phi_P}$. The integral above, therefore, must be split into separate integrals for intervals $0<E<E_c$ and $E>E_c$. In the first interval one needs $J_{\rm env}(E)$, which involves the structure of the potential in a narrow radial range. Since the envelope is tangent to both r_0 and r_1 lines, a simple but accurate approximation for $J_{\rm env}(E)$ can be readily obtained without actually knowing $\Phi(r)$

$$J^2_{\rm env}(E)=J^2_{r_1}(E)-\frac{2m_e(r_1^2e\Phi_1-r_0^2e\Phi_0)^2}{r_1^2e\Phi_1-r_0^2e\Phi_0+(r_0^2-r_1^2)E}. \tag{16}$$

We still need to solve Eq. (2) because the values r_0, Φ_0, r_1, and Φ_1 are unknown and depend on the entire potential structure.

In Eq. (5) for the electron density we use (13a) and (13b) for $J_R^*(E)$, and appropriate expressions for $J_r^*(E)$ at different r values or ranges. First, the quasineutrality relation $N_e=N_i$ at point 0, with $J_r^*(E)$ taken from (9), yields

$$\exp\left(-\frac{e\Phi_0}{kT_i}\right)=1-\int_0^\infty\frac{dE}{\pi kT_e}\exp\left(\frac{-E}{kT_e}\right)\sin^{-1}\frac{J_R^*(E)}{J_{r_0}(E)}. \tag{17}$$

Again, the quasineutrality relation at point 1, with $J_r^*(E)$ from (12), yields

$$\exp\left(-\frac{e\Phi_1}{kT_i}\right)=\int_0^\infty\frac{dE}{\pi kT_e}\exp\left(\frac{-E}{kT_e}\right)\times\left[2\sin^{-1}\frac{J_{\rm env}(E)}{J_{r_1}(E)}-\sin^{-1}\frac{J_R^*(E)}{J_{r_1}(E)}\right]. \tag{18}$$

Since Eq. (12) holds in some neighborhood of point 1, the derivative of the quasineutrality relation with respect to Φ at r_1 (where $dr/d\Phi$ vanishes) finally gives

$$\exp\left(\frac{-e\Phi_1}{kT_i}\right)=\int_0^\infty\frac{T_i\exp(-E/kT_e)dE}{2\pi T_e(E+e\Phi_1)}\times\left[2\frac{J_{\rm env}(E)}{\sqrt{J^2_{r_1}(E)-J^2_{\rm env}(E)}}-\frac{J_R^*(E)}{\sqrt{J^2_{r_1}(E)-J_R^{*2}(E)}}\right]. \tag{19}$$

Note that the integrals in Eqs. (17)–(19) [and later integrals also involving $J_R^*(E)$] must each be split into energy ranges below and above E_c, as with (15). Those equations, together with the relation defining E_c

$$J_{\rm env}(E_c)=J_R(E_c)\approx J_R(0), \tag{20}$$

serve to determine $e\Phi_0/kT_i$, $e\Phi_1/kT_i$, $\sigma_1\equiv e\Phi_PR^2/kT_ir_1^2$, and r_1/r_0 as functions of T_e/T_i and E_c/kT_e. Equation (15) now gives

$$I/I_{\rm OML}=\text{a function of } \quad T_e/T_i, \quad E_c/kT_e. \tag{15$'$}$$

One could then obtain $e\Phi_0/kT_i$, $e\Phi_1/kT_i$, σ_1, and r_1/r_0 as functions of T_e/T_i and $I/I_{\rm OML}$.

Since the quasineutral solution is singular at r_1, the left-hand-side of Eq. (2) must be retained in a thin layer above point 1 in Fig. 1, with charge densities expanded around point-1 values.[9] At a radius r_2 close to r_1 the potential itself blows up to infinity, requiring a second nonquasineutral thin layer that just allows a smooth match to the solution in the broad region reaching to the probe. An analysis of the first layer as in Ref. 9 yields

$$\sigma_2=\sigma_1\left[1+6.9\left(\frac{2\sigma_1^2}{\lambda\mu}\right)^{1/5}\left(\frac{\lambda_{\rm Di}}{R}\right)^{4/5}\left(\frac{kT_i}{e\Phi_P}\right)^{2/5}\right], \tag{21}$$

with $\sigma_2\equiv\sigma_1\times r_1^2/r_2^2$, and μ and λ new functions of T_e/T_i and E_c/KT_e

$$\mu \equiv \int_0^\infty \frac{dE}{\pi k T_e} \exp\left(\frac{-E}{kT_e}\right) \left[\frac{2J_{\rm env}(E)}{\sqrt{J_{r_1}^2(E) - J_{\rm env}^2(E)}} - \frac{J_R^*(E)}{\sqrt{J_{r_1}^2(E) - J_R^{*2}(E)}} \right], \tag{22}$$

$$\lambda \equiv -\exp\left(-\frac{e\Phi_1}{kT_i}\right) + \int_0^\infty \frac{kT_i^2 dE \exp(-E/kT_e)}{4\pi T_e (E + e\Phi_1)^2} \times \left[2J_{\rm env}(E) \frac{3J_{r_1}^2(E) - 2J_{\rm env}^2(E)}{(J_{r_1}^2(E) - J_{\rm env}^2(E))^{3/2}} - J_R^*(E) \frac{3J_{r_1}^2(E) - 2J_R^{*2}(E)}{(J_{r_1}^2(E) - J_R^{*2}(E))^{3/2}} \right]. \tag{23}$$

In the broad region above the thin layers we take $e\Phi \gg e\Phi_1 \sim kT_i$, $e\Phi \gg E \sim kT_e$ (Fig. 1), making N_i/N_∞ negligibly small in Eq. (2). Also, since r-lines now lie far to the right in Fig. 2 throughout most of this region, we simplify the integral for N_e/N_∞ in (5) by using Eq. (12) and the approximations $J_R^*(E) \sim J_{\rm env}(E) \ll J_r(E)$, $J_r(E) \approx J_r(0)$, leading to

$$\frac{N_e}{N_\infty} \approx \frac{\kappa}{\pi} \frac{R}{r} \sqrt{\frac{\Phi_P}{\Phi}}, \tag{24}$$

$$\kappa \equiv \int_0^\infty \frac{dE}{kT_e} \exp\left(\frac{-E}{kT_e}\right) \left[2\frac{J_{\rm env}(E)}{J_R(0)} - \frac{J_R^*(E)}{J_R(0)} \right], \tag{25}$$

with κ again a function of T_e/T_i and E_c/kT_e. Note that use of $J_r(E) \approx J_r(0)$ and (12) fails near r_1 and R respectively, overestimating N_e, whereas taking J_R^*/J_r and $J_{\rm env}/J_r$ small underestimates N_e and fails near both r_1 and R. In the $R = R_{\max}$ $[J_R^*(E) = J_R(E)]$ case of Ref. 9 the exact value for $N_e(r=R)$ in Eq. (5) is $(1/2)N_\infty$, while the approximation in Eq. (24) gives $N_\infty \times \kappa/\pi$, which Fig. 5(b) of Ref. 9 shows to be about N_∞ (for $T_e = T_i$); a net overestimate of N_e increases shielding and leads to an underestimate of both $R_{\max}$ and $I/I_{\rm OML}(R > R_{\max})$. Clearly, the error will be greater the lower the bias.[12]

Using $N_i = 0$ and Eqs. (24) and (25) in (2), and defining

$$u \equiv \ln\frac{r_2}{r}, \quad g \equiv \left[\pi \frac{\sqrt{\sigma_2}}{\kappa} \frac{\lambda_{\rm Di}^2}{R^2} \frac{kT_i}{e\Phi_P} \right]^{2/3} \frac{e\Phi}{kT_i},$$

Poisson's equation, and the boundary conditions imposed by matching to the second layer, become

$$\frac{d^2 g}{du^2} = \frac{e^{-u}}{\sqrt{g}}, \quad g = \frac{dg}{du} = 0 \quad \text{at} \quad u = 0 \quad (g \propto u^{4/3}).$$

From the numerical solution for $g(u)$ one finds $\Phi(r)$; the boundary condition $\Phi = \Phi_P$ at $r = R$ then yields

$$g\left[\ln\left(\sqrt{\frac{e\Phi_P}{kT_i \sigma_2}} \right) \right] = \left(\frac{\pi^2 \sigma_2}{\kappa^2} \right)^{1/3} \left(\frac{\lambda_{\rm Di}}{R} \right)^{4/3} \left(\frac{e\Phi_P}{kT_i} \right)^{1/3}. \tag{26}$$

Using (21) in (26) determines a last relation

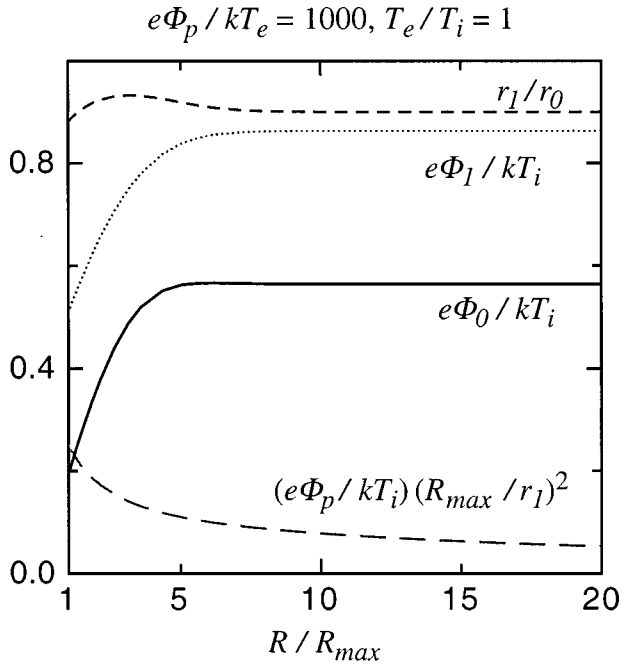

FIG. 3. Dimensionless ratios $e\Phi_0/kT_i$, $e\Phi_1/kT_i$, $\sigma_1 R_{\max}^2/R^2 \equiv e\Phi_P R_{\max}^2/kT_i r_1^2$, and r_1/r_0 vs $R/R_{\max}$, for $T_e/T_i = 1$ and $e\Phi_P/kT_e = 1000$; results for $e\Phi_P/kT_e = 300$ and 3000 are quite similar.

$$\frac{E_c}{kT_e} = \text{a function of} \quad \frac{T_e}{T_i}, \frac{\lambda_{\rm Di}}{R}, \frac{e\Phi_P}{kT_i}. \tag{27}$$

Equations (15′) and (27) give $I/I_{\rm OML}$ versus $e\Phi_P/kT_e$, $R/\lambda_{\rm De}$, and T_e/T_i.

The $R = R_{\max}$ limit studied in Ref. 9 corresponds to $E_c = 0$, Eq. (15) or (15′) then giving $I = I_{\rm OML}$. Using (16), Eq. (20) would read $J_{\rm env}(0) = J_R(0)$ or $r_0^2\Phi_0 = R^2\Phi_P$ (point 0 on the diagonal of Fig. 1); this condition, together with Eqs. (17)–(19), determined σ_1, $e\Phi_1/kT_i$, and $e\Phi_0/kT_i$ $(= \sigma_1 r_1^2/r_0^2)$ as functions of just T_e/T_i. With μ, λ, and κ functions of T_e/T_i too, Eq. (27) gave $R_{\max}/\lambda_{\rm De}$ versus $e\Phi_P/kT_e$ and T_e/T_i (Fig. 7 in Ref. 9).

For completeness, we now consider briefly the OML regime $(R/R_{\max} \leqslant 1)$, which is naturally of less interest because the current is known, $I = I_{\rm OML}$. For the non-OML conditions we have studied until now, the potential profile below point 0 in Fig. 1 [which was determined by the equation $N_i = N_e$ with $J_r^*(E) = J_r(E)$ in (5)] varied with $J_R^*(E)$, and thus with $R/R_{\max}$. In the OML regime, however, we have $J_R^*(E) = J_R(E)$, and thus a single profile throughout. As $R/R_{\max}$ decreases from unity, point 0 just moves down on that particular profile away from the diagonal, with $R^2\Phi_P/r_0^2\Phi_0$ decreasing too. For specified T_e/T_i and $R^2\Phi_P/r_0^2\Phi_0$ values, Eqs. (17)–(19) would give σ_1, $e\Phi_1/kT_i$, $e\Phi_0/kT_i$, and r_1/r_0; then (22), (23), and (25) give μ, λ, and κ. Finally, using (21) in (26) would yield $R^2\Phi_P/r_0^2\Phi_0$ versus $R/\lambda_{\rm De}$, T_e/T_i, and $e\Phi_P/kT_e$.

IV. DISCUSSION OF RESULTS

Figure 3 shows $e\Phi_0/kT_i$, $e\Phi_1/kT_i$, r_1/r_0 and $e\Phi_P R_{\max}^2/kT_i r_1^2$ $(\equiv \sigma_1 R_{\max}^2/R^2)$ versus $R/R_{\max}$ at $T_e/T_i = 1$ and $e\Phi_P/kT_e = 1000$; $\sigma_1 R_{\max}^2/R^2$ was plotted because σ_1

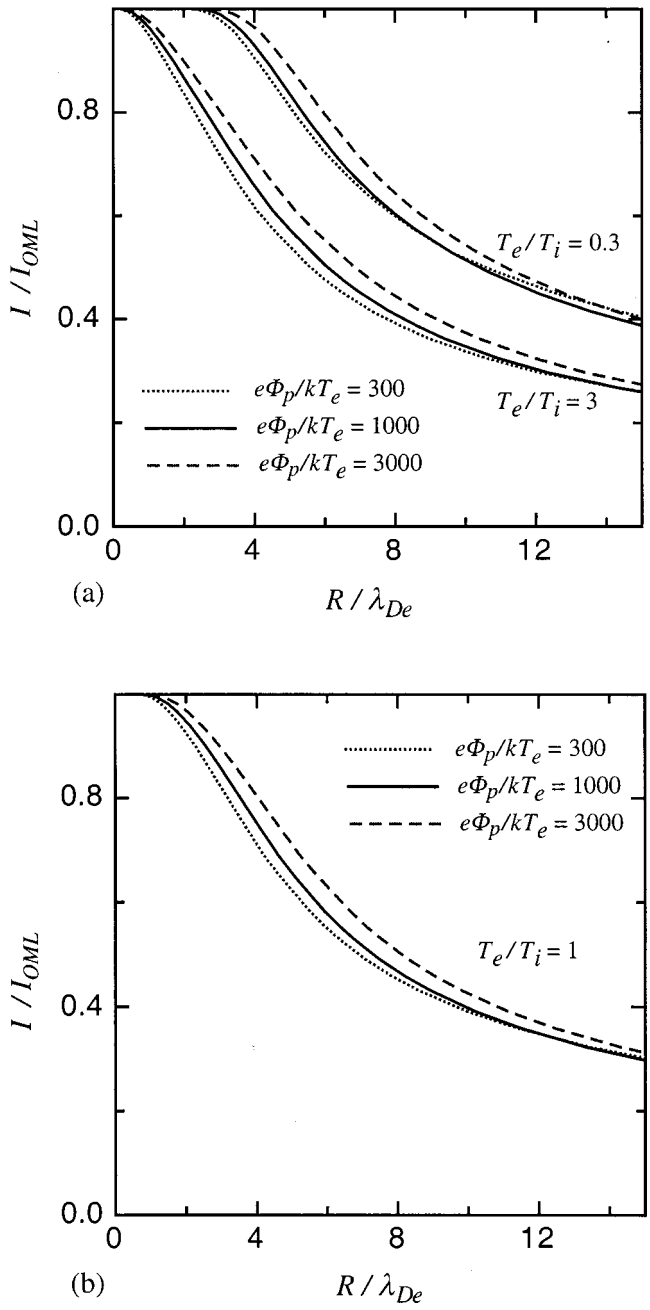

FIG. 4. Current ratio I/I_{OML} vs R/λ_{De} for a few values of $e\Phi_P/kT_e$ and (a) $T_e/T_i=0.3$ and 3, (b) $T_e/T_i=1$.

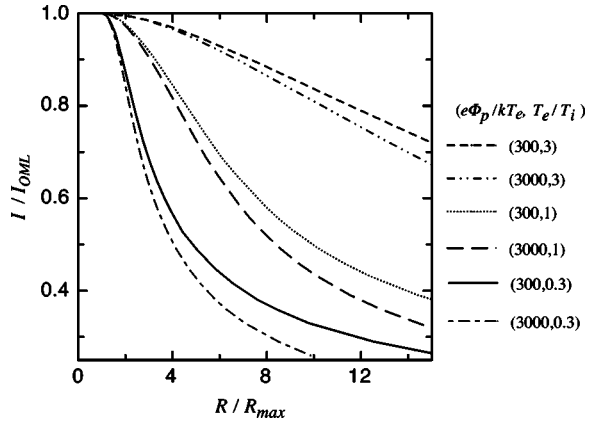

FIG. 5. Current ratio I/I_{OML} vs R/R_{max} for a few values of $e\Phi_P/kT_e$ and T_e/T_i.

gets too large. As suggested by other results below, values for $e\Phi_P/kT_e=300$, 1000, and 3000 are quite close to each other. Actually, as noted in Sec. III, plots in Fig. 3 would be fully $e\Phi_P/kT_e$-independent if I/I_{OML} replaced R/R_{max}.

Figures 4(a) and 4(b) give I/I_{OML} versus R/λ_{De} for a few values of T_e/T_i and $e\Phi_P/kT_e$. Note that the dependence on probe bias is indeed very weak. We also note that previous asymptotic results on the limit $R/\lambda_{\mathrm{De}}\to\infty$, at $T_e/T_i=1$, showed I/I_{OML} to approach a limit value that decreased with increasing $e\Phi_P/kT_e$,[13] ($I/I_{\mathrm{OML}}\to 1.29kT_e/e\Phi_P$, here being 0.075, 0.041, and 0.024 for $e\Phi_P/kT_e=300$, 1000, and 3000, respectively). Crossover points for the curves can be seen in Figs. 4(a) and 4(b), however. The asymptotic approach is very slow;[13] as a check, we found a value $I/I_{\mathrm{OML}}=0.057$ at $R/\lambda_{\mathrm{De}}=393$ for $e\Phi_P/kT_e=1000$, and at $R/\lambda_{\mathrm{De}}=209$ for $e\Phi_P/kT_e=3000$.

Note that curves in Figs. 4(a) and 4(b) can roughly be obtained from each other by a horizontal displacement that is T_e/T_i-dependent. Hence, the dependence on R/λ_{De} and T_e/T_i can be approximated by a simple law that should be useful for design considerations,

$$\frac{I}{I_{\mathrm{OML}}}\approx G\left(\frac{R-R_{\mathrm{max}}}{\lambda_{\mathrm{De}}}\right)=G\left(\frac{R}{\lambda_{\mathrm{De}}}-\tilde{R}_{\mathrm{max}}\left(\frac{T_e}{T_i}\right)\right). \tag{28}$$

Here $\tilde{R}_{\mathrm{max}}\equiv R_{\mathrm{max}}/\lambda_{\mathrm{De}}$ is roughly a decreasing function of the ratio T_e/T_i, as determined in Ref. 9, and G is some universal function obtained from the figures [$G(0)=1$, G decreasing with increasing positive argument]. Writing the argument of G as $(R/R_{\mathrm{max}}-1)\times\tilde{R}_{\mathrm{max}}$, it follows that I/I_{OML} drops faster with R/R_{max} the higher $\tilde{R}_{\mathrm{max}}$, i.e., the lower T_e/T_i. This can be seen clearly in Fig. 5, showing I/I_{OML} versus R/R_{max}.

The present results lead to simple design conclusions: One might reasonably use tether radii over a sensible range beyond R_{max}; this range exceeds λ_{De} even if R_{max} is well below λ_{De} (the high-T_e/T_i case); in terms of the ratio R/R_{max}, the range increases rapidly with decreasing R_{max}. These conclusions are relevant for standard applications of bare tethers, which find a plasma with Debye length and, to some degree, ratio T_e/T_i, varying along the orbit. These comments apply with even more force if the tether is used for orbit raising or lowering due to the large variations of plasma density with altitude.

The conclusions may also serve in discussing the effect of a plasma velocity U relative to the probe. This introduces a new characteristic ion (ram) energy, which, for a tether orbiting in the F layer, where O^+ is the dominant ion species, is large compared with the thermal energy, $(1/2)m_iU^2\approx 4.5\,\mathrm{eV}\gg kT_i\sim 0.15\,\mathrm{eV}$. Note that this is not the case at higher altitudes, where H^+ ions are dominant—and U^2 is somewhat reduced. In the F-layer the unperturbed ion distribution function would be strongly nonisotropic, and the electric field nonradial.

The OML current law, however, is still valid, being independent of both ion distribution function and cross-section shape [just replace $2R$ with $perimeter/\pi$ in Eq. (1)];[8] the law does not require a rotationally symmetric potential.[9] The law just requires that the unperturbed electron distribution function be isotropic, a condition well satisfied in our case, with $(1/2)m_eU^2 \ll kT_e$; the high-bias limit law (1) is specially robust: It holds independently of that particular isotropic distribution. The effect of a large ion ram energy would then be a change in the domain of validity for the OML law.

We now recall that I/I_{OML} remains unity over some (and close to unity over a much larger) parametric domain, mirroring the fact that $I_{\mathrm{OML}}/I_{\mathrm{th}}$ in (1) is independent of R/λ_{De} and T_e/T_i. This means that one could alter substantially T_i, or the probe cross section (keeping its perimeter), thus fully modifying the structure of the potential field, without reaching the boundary of the domain of OML validity, that is, with no current variation. This is a case quite the opposite of large spherical electron collectors as used in conductive tethers previously flown. In predicting the new domain of validity (instead of an actual value for I) one might use crude models if conservative, although definite conclusions on this point must wait for a more careful analysis

For the conditions of interest, $e\Phi_P \gg (1/2)m_iU^2$, ions would be kept far away from the probe for all directions, with some (angle-dependent) potential structure similar to that shown in Fig. 1. In a crude model, one would ignore the nonthermal character of the ram energy, except for the fact that it makes the ion characteristic energy angle-dependent. In a plasma with $T_i \sim T_e$, one should have effective ion temperatures $kT_i(\mathrm{eff}) \sim (1/2)m_iU^2 \sim 30kT_e$ on the windward side, $T_i(\mathrm{eff}) \sim T_e$ on the lateral sides, and, as argued below, $T_i(\mathrm{eff}) \sim T_e \times \sqrt{2kT_e/m_iU^2} \sim 0.2T_e$, on the lee side. Figure 4(a), showing $I/I_{\mathrm{OML}} > 0.95$ at $R = \lambda_{\mathrm{De}}$, for T_e/T_i as high as 3, then suggests that a probe of radius $R < \lambda_{\mathrm{De}}$ would collect current close to the OML value. Our estimate for $T_i(\mathrm{eff})$ on the lee side is based on the fact that, for other parameters fixed, the minimum distance reached by the ions, r_1 in Fig. 1, depends on the characteristic ion energy;[9] we then took $r_1 \sim R\sqrt{e\Phi_P/kT_i}\sqrt{T_e/T_i}$ for T_e/T_i large or about unity, from the zero-U, $R = R_{\max}$ analysis of Ref. 9, and $r_1(\mathrm{lee}) \sim r_1(\mathrm{lateral}) \times \sqrt{m_iU^2/2kT_e}$ from simple wake considerations.

ACKNOWLEDGMENT

The work of J.R.S. was supported by the Comisión Interministerial de Ciencia y Tecnología de Spain under Grant No. PB97-0574-C04-1. The work of R.D.E. was supported by NASA Grant No. NAG8-1605.

[1] M. Martínez-Sanchez and D. H. Hastings, J. Astronaut. Sci. **35**, 75 (1987).
[2] R. D. Estes, E. Lorenzini, J. R. Sanmartín, J. Pelaez, M. Martínez-Sanchez, L. Johnson, and I. Vas, J. Spacecr. Rockets **37**, 205 (2000).
[3] R. D. Estes, J. Geophys. Res. **93**, 945 (1988); J. R. Sanmartín and M. Martínez-Sanchez, *ibid.* **100**, 1677 (1995).
[4] J. R. Sanmartín and R. D. Estes, J. Geophys. Res. **102**, 14625 (1997).
[5] M. Martínez-Sanchez and J. R. Sanmartín, J. Geophys. Res. **102**, 27257 (1997).
[6] J. R. Sanmartín, M. Martínez-Sanchez, and E. Ahedo, J. Propul. Power **9**, 353 (1993).
[7] R. D. Estes, J. R. Sanmartín, and M. Martínez-Sanchez, J. Spacecr. Rockets **37**, 197 (2000).
[8] J. G. Laframboise and L. W. Parker, Phys. Fluids **16**, 629 (1973).
[9] J. R. Sanmartín and R. D. Estes, Phys. Plasmas **6**, 395 (1999).
[10] L. W. Parker and E. C. Whipple, Jr., Ann. Phys. (N.Y.) **44**, 126 (1967).
[11] Condition $E_{\mathrm{env}}(r) = 0$ in (11b) corresponds to a minimum of $r^2\Phi$ (the profile tangent at point 0, when reached from above, crosses the origin in Fig. 1). The quasineutral solution has no such property reaching 0 from below, and breaks down there; use of the full Eq. (2), however, would locally round the profile with no effect beyond the immediate neighborhood of 0, which just appears as the no energy-barrier point closest to 1.
[12] Results for $R_{\max}$ from our analytical approach can be compared to numerical computations by Laframboise, who considered $e\Phi_P/kT_e$ of order unity or moderately large [National Technical Information Service Document No. 634596 (J. G. Laframboise, ''Theory of spherical and cylindrical Langmuir probes in a collisionless, Maxwellian plasma at rest,'' University of Toronto Institute for Aerospace Studies Report No. 100, 1966); copies may be ordered from the National Technical Information Service, Springfield, VA 22161]. Figures 42 and 50(b) in Laframboise's work give $R_{\max} \approx 0.96\lambda_{\mathrm{De}}$ at $T_e = T_i$ and the highest bias, $e\Phi_P/kT_e = 25$; Figs. 6 and 7 of Ref. 9 give $R_{\max} \approx 0.77\lambda_{\mathrm{De}}$, or about 20% too low, at the same conditions. Differences are greater at still lower bias, $e\Phi_P/kT_e = 20$ or 15.
[13] M. J. M. Parrot, L. R. O. Storey, L. W. Parker, and J. G. Laframboise, Phys. Fluids **25**, 2388 (1982).